Torsional oscillations within a magnetic pore in the solar photosphere

Stangalini, Marco; Erdélyi, Robertus; Boocock, Callum; Tsiklauri, David; Nelson, Christopher J.; Del Moro, Dario; Berrilli, Francesco; Korsós, Marianna B.

Published in:
Nature Astronomy

DOI:
10.1038/s41550-021-01354-8

Publication date:
2021

Citation for published version (APA):
Stangalini, M., Erdélyi, R., Boocock, C., Tsiklauri, D., Nelson, C. J., Del Moro, D., Berrilli, F., & Korsós, M. B. (2021). Torsional oscillations within a magnetic pore in the solar photosphere. *Nature Astronomy*, *5*(7), 691-696. https://doi.org/10.1038/s41550-021-01354-8

Torsional Oscillations in a Solar Magnetic Pore Observed by IBIS

M. Stangalini[1,2,], R. Erdélyi[3,4,5], C. Boocock[6], D. Tsiklauri[6], C. J. Nelson[7], D. Del Moro[8], F. Berrilli[8], M. B. Korsós,[9,3,4]*

(1) ASI, Italian Space Agency, Via del Politecnico snc, 00133, Rome, Italy
(2) INAF-OAR, National Institute for Astrophysics, Via Frascati, 33, 00078, Monte Porzio Catone (RM), Italy
(3) Solar Physics and Space Plasma Research Centre (SP2RC), School of Mathematics and Statistics, The University of Sheffield, Sheffield, S3 7RH, UK
(4) Department of Astronomy, Eötvös Loránd University, Budapest, Pázmány P. sétány 1/A, H-1117, Hungary
(5) Gyula Bay Zoltán Solar Observatory (GSO), Hungarian Solar Physics Foundation (HSPF), Petőfi tér 3., Gyula, H-5700, Hungary
(6) School of Physics and Astronomy, Queen Mary University of London, Mile End Road, London, E1 4NS, UK
(7) Astrophysics Research Centre (ARC), School of Mathematics and Physics, Queen's University, Belfast, BT7 1NN, N. Ireland, UK
(8) Department of Physics, University of Rome Tor Vergata, Via delle Ricerca Scientifica 1, 00133, Rome, Italy
(9) Department of Physics, Aberystwyth University, Ceredigion, Cymru, SY23 3BZ, UK

Abstract

Alfvén waves have proven important in a range of physical systems (e.g., stars, planetary atmospheres, tokamaks) due to their ability to transport non-thermal energy over long distances in a magnetised plasma. This property is of specific interest in solar physics where the extreme heating of the solar atmosphere remains unexplained. Despite several claims in the upper layers of the Sun's atmosphere their direct signature, torsional oscillations of magnetic iso-contours, is yet to be observed. This is because detecting signatures of torsional oscillations in a magnetic structure with high-enough sensitivity remains a challenge. Here, we report the detection of anti-phase torsional oscillations of the circular polarisation (a proxy for the line-of-sight magnetic field) measured in a magnetic pore in the photosphere of the Sun. Supporting state-of-the-art simulations are in agreement with observations and provide hints on the excitation mechanism of these waves.

The search for torsional oscillations in magnetic structures in the lower solar atmosphere was the main focus of a number of studies in recent years [Mathioudakis et al.]. Most of them were focused on the identification of Alfvén waves, incompressible plasma perturbations which have magnetic tension as their sole restoring force.

Their existence was predicted theoretically more than 70 years ago [1] and they have recently become the main focus of a number of studies in solar physics that resulted in a range of indirect confirmations of its existence. These studies have been limited mostly to the upper solar atmosphere and solar wind, meaning despite their apparent importance, Alfvén waves have never been *directly detected* in the solar photosphere. This means they represent the most elusive, yet physically intriguing, class of magnetohydrodynamic (MHD) waves waiting to be fully identified.

In magnetic flux tubes, Alfvén waves manifest as either axisymmetric or anti-symmetric torsional perturbations [2]. After their discovery, Alfvén waves were immediately recognized for their potential impact in many research areas, including neutrino physics [3], the heating of the solar upper atmosphere - the corona - to million-degree temperatures [4,5,6], proto-stellar disks [7], the physics of the interstellar medium [8], particle acceleration around supermassive black holes [9], and nuclear fusion research, where these magnetic waves have been proposed as a possible effective heating mechanism in tokamaks [10,11]. So far, despite the many suggestions of the presence of Alfvén waves in the upper layers of the solar atmosphere [12,13,14,15] and in the solar wind [16], no observation of torsional motion that could be linked to TAWs [17] has been reported in the photosphere.

One of the fundamental major applications in plasma physics is that torsional waves play a key role in the energy transportation, heating and energy dissipation. Examples include both laboratory and space plasmas such as the solar atmosphere from the chromosphere to the corona, the intergalactic medium, or plasma fusion

reactors. In this article, we present the detection of non-axisymmetric torsional oscillations in a compact photospheric magnetic structure, made possible by high-resolution observations acquired by the IBIS 2D spectropolarimeter at the Dunn Solar Telescope (DST, New Mexico, USA) [18].

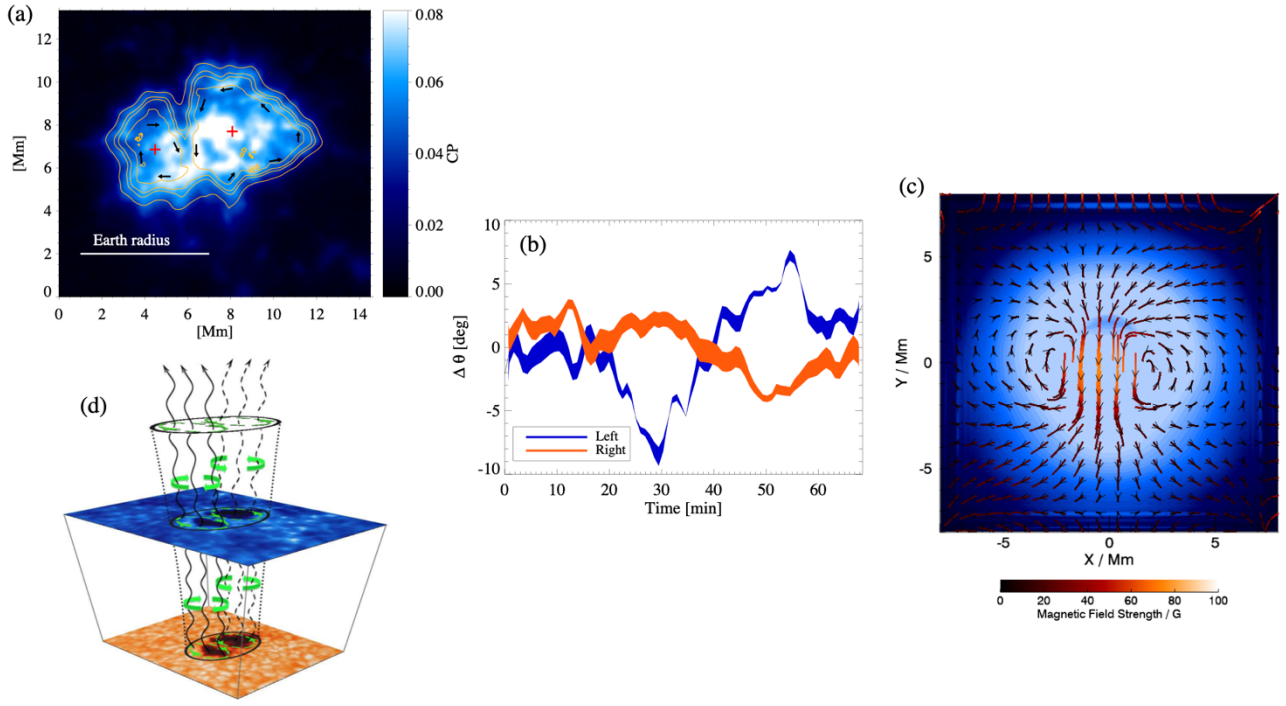

Figure 1. Detection of torsional oscillations in a compact magnetic structure in the solar photosphere. *(a) Circular Polarization map of the magnetic pore observed by IBIS@DST. (b) Measured angular rotation oscillations of the two lobes of the magnetic pore, as obtained from a cross-correlation tracking analysis at the edges of the flux tube. (c) Supplementary numerical simulation showing horizontal magnetic field perturbations for the m=1 torsional Alfvén wave over a contour of the magnetic field strength. (d) Cartoon depicting the m=1 anti-symmetric torsional Alfvén oscillations in solar context.*

Results

Spectropolarimetry has long been a standard method used to measure magnetic fields in the Sun and other stars; however, the spatial, temporal, and spectral resolutions we can now achieve with observations of our nearest star means the polarimetric footprint left by the magnetic field in the Sun's photospheric plasma can now be exploited to map and study its magnetic structures and their associated dynamics in fine detail. Specifically, the high temporal and spatial resolutions (scales close to 120 km on the surface of the Sun can be sampled a few times every minute) achieved by modern 2D solar spectro-polarimetric imagers such as IBIS, are perfect for studying the fine-structure and rapid dynamical behaviour of photospheric magnetic structures such as pores. The instantaneous circular polarization map of the light emerging from the pore studied here in the magnetically sensitive *Fe I* 617.3 nm spectral line is plotted in Fig. 1 (panel a). This represents a direct indicator of the vertical magnetic field of the structure at this time. The ~69 min duration and 52 s temporal resolution of the IBIS dataset studied here allow us to investigate the evolution of the entire magnetic structure and, specifically, to trace torsional magnetic oscillations, perpendicular to the line-of-sight, through time. To achieve this aim, we initially transform the temporal sequence of circular polarization maps into polar coordinates (see Fig. S1 for an example). The approximate position of the centres of the two magnetic lobes (marked by the two red crosses in Fig. 1 panel a) are employed as the radial origins of the structures. Over-plotted on Fig. 1 (panel a) are the streamlines of the torsional oscillations indicating its $m = 1$ dipolar nature. The measured angular shifts of both lobes, as a function of time, are shown in Fig. 1 (panel b), where it is simple to recognize a periodic angular displacement in both sides of the pore. It is worth noting that the torsional oscillations of the two lobes are out of phase. The thickness of the curves indicates the 3σ error associated with the measures (see Appendix for more details).

A series of supporting 3D MHD simulations were performed using Lare3d [19] to demonstrate a possible formation mechanism for m =1 TAWs in the lower solar atmosphere. Similar to [32], these simulations show the excitation of TAWs as a result of coupling with kink oscillations. Lare3d is a Lagrangian remap code that solves the resistive MHD equations over a 3D staggered grid [20]. A high-density, vertically stratified, divergent, flux tube was placed at the centre of the domain, representing the magnetic pore, and linear Alfvén waves are then driven from the lower boundary, modeling the observed photospheric surface. It is found that the investigated magnetic flux tube exhibits structural non-axisymmetric torsional oscillations, manifesting as periodic non-axisymmetric rotation of the two lobes composing the magnetic structure. The rotation of the magnetic fields at a height of 500 km above the photosphere is shown in Fig. 1 (panel c). These supplementary, state-of-the-art numerical simulations show underpinning evidence for the presence of anti-symmetric magnetic field and plasma velocity oscillations that, similar to [32], are consistent with m=1 torsional Alfvén waves within a model solar photospheric magnetic structure(a cartoon depiction is plotted in Fig. 1 panel d). The two counter-rotating oscillations in the velocity and magnetic fields are readily identifiable in Figs. S6 and S7. These supporting visualisations were developed to highlight the dynamics of these oscillations, with movies being presented in the Supplementary Material. At the density inhomogeneity at the edge of the flux tube, transverse wave modes are coupled to the m =1 torsional Alfvén mode similar to the coupling of kink modes to the m =1 Alfvén mode described in [21]. The typical result shown here demonstrates the formation of two counter-rotating oscillations either side of the flux tube.

The power spectra of the velocity torsional oscillations in the observed pore are shown in Fig. 2 (panel a). In the same plot, we show the confidence levels as estimated from a bootstrapping randomization test making use of 1000 runs (see Appendix for more details). Several harmonics with confidence levels larger than 95% are seen in the spectra of the two lobes. In Fig. 2 (panel b), we show the scaling law of the peaks found in the right lobe, as obtained from a multi-Gaussian fit to the spectrum. The power spectra of the torsional oscillations of the two lobes exhibit several peaks consistent with harmonics of standing oscillations. We note that the presence of harmonics rules out the possibility that the observed torsional oscillations might be the results of noise or seeing effects. The fit to the data yields fundamental frequency $\nu_f = 0.65 \pm 0.02$ mHz, corresponding to a period of about 25 min.

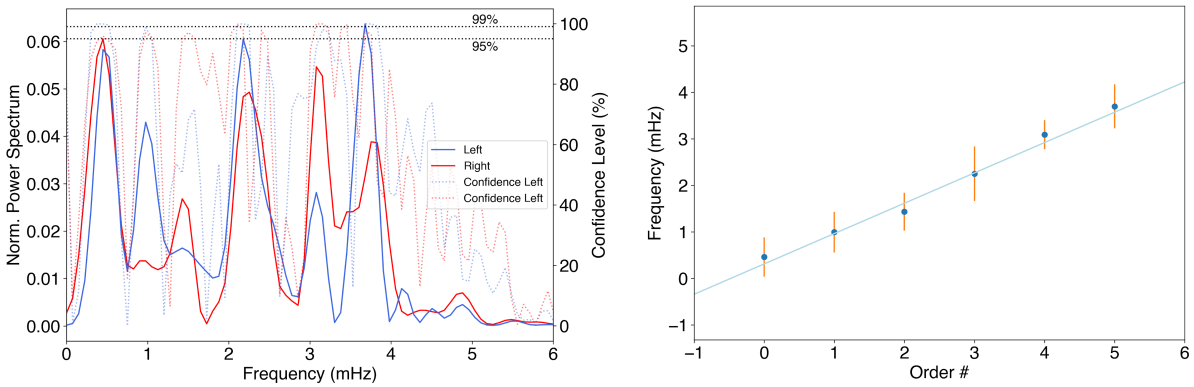

Figure 2. Power spectrum of the torsional oscillations and harmonics.
Power spectrum of the torsional velocity of the two lobes (left) showing the presence of several peaks, scaling as harmonics (right, see Supplementary Material for more details). The average of the velocity time series is subtracted and the time series themselves are normalized by their standard deviation before estimating the power spectrum. On the same plot we also show the confidence levels as obtained by a bootstrapping randomization test with 1000 runs.

Next, in order to provide a first insight into the associated Alfvén wave energy flux, we make use of the following relation,

$$E = \rho v^2 c_A, \quad (1)$$

where ρ is the mass density, v the velocity of oscillation, and c_A the Alfvén wave phase speed. Substituting the average magnetic field obtained from the COG method [22] in the annular regions, and the average values of the density as estimated from spectropolarimetric inversions (see Appendix), into this equation we have an estimate of the energy content of the two lobes. Given the measured value of the root mean square velocity amplitude of the torsional oscillations ($v_{left} \sim 0.4$ km s^{-1} and $v_{right} \sim 0.3$ km s^{-1}), the estimated energy flux is $E_{left} = 135 \pm 85$ kW/m^2 and $E_{right} = 140 \pm 80$ kW/m^2 for the two lobes, respectively. These values are in excess

of the required energy flux needed to heat the active region chromosphere (~ 20 kW m^{-2}) and corona (~ 10 kW m^{-2}) [23]. This implies that, in the upper limit regime (lower error bound) ~50% of the total estimated energy would need to be dissipated to heat the active region chromosphere and corona. This energy content is therefore quite large with respect to the required value, however, it is worth noting that not all the energy contained in the waves may be transported to the upper atmosphere or converted to thermal energy at those heights. We note that the above estimates of the energy flux are only applicable to a single, fixed frequency. If, instead of a single frequency, a wide spectrum is considered, commensurately, more heating can be provided as is shown in [e.g., 20, 21] .

Discussion

Obtaining long-duration excellent quality data, like those used in this work, is generally hampered by the large variability of daytime seeing conditions. For this reason, it is difficult to judge how ubiquitous these torsional motions can be, and whether they are the key to a steady heating mechanism of the chromosphere and corona. We would also like to comment on some alternative interpretation. In particular, Goossens et al. [] have shown that kink waves can also generate velocity fields that are spatially and temporally varying sums of both transverse and rotational motion. With other words, such bulk transverse motions in flux tubes also have omnipresent rotational motions that actually may appear similar to those in our observations and simulations that *we* interpret as *m*=1 TAW. While other authors have interpreted a similar behavior as a coupling and excitation mechanism of TAWs, we find this is an interesting alternative to be considered. However, the transverse dynamics of density structure in the case of m=1, fast kink wave (the 1st branch) [36] is significantly different from our observations and MHD simulations, hence providing support for our TAW interpretation.
Our simulations therefore demonstrate that TAWs can actually be excited in the solar photosphere and may constitute an effective mechanism for extracting energy from the solar photosphere.
Regarding the possible damping mechanisms of torsional Alfvén waves, one such process expected to occur in the solar plasma is phase mixing [13,23]. In flux tube geometry, this requires a varying background Alfvén speed in the radial direction, i.e., perpendicular to the tube axis. Since the magnetic field strength does indeed change as a function of radius in the pore, there will also be a varying Alfvén speed, enabling the necessary conditions for phase mixing to take place. This process may cause the torsional velocity perturbations in neighbouring streamlines to go out-of-phase with height, allowing the possibility of the development of Kelvin-Helmholtz instability [4], thus generating smaller length scales at which plasma heating becomes more efficient [e.g., 24]. Higher in the atmosphere, for example, in the corona, the resultant sub-resolution incoherent motions due to these processes could contribute significantly to observed non-thermal line widths, which are known to be much greater in magnitude than actual resolved Doppler velocities [e.g., 25].
We would like to stress that our supporting numerical simulations indicate that when a (vertical) magnetic flux tube is driven at the bottom with a linearly polarized Alfvén wave with frequencies similar to Alfvén or below, then the generated *m*=1 torsional Alfvén wave is persistently excited. At the density inhomogeneity within the umbra of the flux tube transverse wave modes are coupled to the *m* =1 torsional Alfvén mode through e.g. resonant damping similar to the coupling of kink modes to the *m* =1 Alfvén mode described in [21]. A typical result of such numerical modelling shown here demonstrates the formation of two counter-rotating oscillations either side of the flux tube. These supplementary numerical simulations are not in any way contrived. On the contrary, the described process of *m*=1 TAW mode excitation is a natural process and is expected to be ubiquitous in the solar photosphere.

Data availability: Raw IBIS can be provided on request.

References

[1] H. Alfvén. Nature, 150:405–406, October 1942.
[2] H. C. Spruit. Propagation speeds and acoustic damping of waves in magnetic flux tubes. Sol. Phys., 75:3–17, January 1982.
[3] John N. Bahcall and HA Bethe. Solution of the solar-neutrino problem. Physical Review Letters, 65(18):2233, 1990.
[4] P. K. Browning and E. R. Priest. Kelvin-Helmholtz instability of a phased-mixed Alfven wave. A&A, 131:283–290, February 1984.

[5] Liu, Jiajia, Nelson, Chris J., Snow, Ben, Wang, Yuming, Erdélyi, Robert, Evidence of ubiquitous Alfvén pulses transporting energy from the photosphere to the upper chromosphere, Nature Communications, 3504-10, Aug. 2019, 10.1038/s41467-019-11495-0
[6] R. Erdélyi and V. Fedun. Are There Alfvén Waves in the Solar Atmosphere? Science, 318:1572–, December 2007.
[7] MJ Vasconcelos, V Jatenco-Pereira, and R Opher. Alfvénic heating of protostellar accretion disks. The Astrophysical Journal, 534(2):967, 2000.
[8] Christopher F McKee and Ellen G Zweibel. Alfven waves in interstellar gas dynamics. The Astrophysical Journal, 440:686, 1995.
[9] Toshikazu Ebisuzaki and Toshiki Tajima. Astrophysical zev acceleration in the relativistic jet from an accreting supermassive black hole. Astroparticle Physics, 56:9–15, 2014.
[10] L. Chen and A. Hasegawa. Plasma heating by spatial resonance of Alfvén wave. Physics of Fluids, 17:1399–1403, July 1974.
[11] A. Hasegawa and L. Chen. Kinetic processes in plasma heating by resonant mode conversion of Alfven wave. Physics of Fluids, 19:1924– 1934, December 1976.
[12] A. Hasegawa and L. Chen. Kinetic processes in plasma heating by resonant mode conversion of Alfven wave. Physics of Fluids, 19:1924– 1934, December 1976.
[13] J. Heyvaerts and E. R. Priest. Coronal heating by phase-mixed shear Alfven waves. A&A, 117:220–234, January 1983.
[14] D. B. Jess, M. Mathioudakis, R. Erdélyi, P. J. Crockett, F. P. Keenan, and D. J. Christian. Alfvén Waves in the Lower Solar Atmosphere. Science, 323:1582–, March 2009.
[15] P. Kohutova, E. Verwichte, C. Froment, First direct observation of a torsional Alfvén oscillation at coronal heights, A&A 633 L6 (2020) DOI: 10.1051/0004-6361/201937144
[16] Velli, M., and F. Pruneti. "Alfvén waves in the solar corona and solar wind." Plasma Physics and Controlled Fusion 39.12B (1997): B317.
[17] T. Van Doorsselaere, V. M. Nakariakov, and E. Verwichte. Detection of waves in the solar corona: Kink or Alfvén? The Astrophysical Journal Letters, 676(1): L73, 2008.

[18] F Cavallini. IBIS: A New Post-Focus Instrument for Solar Imaging Spectroscopy. Sol. Phys., 236:415–439, July 2006.
[19] T. D.Arber and A. W. Longbottom and C. L.Gerrard and A. M.Milne A Staggered Grid, Lagrangian Eulerian Remap Code for 3-D MHD Simulations. Journal of Computational Physics, 171(1):151-181, 2001
[20] Tsiklauri D. and Nakariakov V.M., "Wide-Spectrum Slow Magnetoacoustic Waves in Coronal Loops", Astron. Astrophys., 379, 1106-1112 (2001)
[21] Tsiklauri D., "A mechanism for parallel electric field generation in the MHD limit: possible implications for the coronal heating problem in the two stage mechanism", Astron. Astrophys., 455, 1073-1080, (2006)
[22] D. E. Rees and M. D. Semel. Line formation in an unresolved magnetic element - A test of the centre of gravity method. A&A, 74:1–5, April 1979.
[23] M. S. Ruderman, and N Petrukhin, Phase mixing of Alfvén waves propagating in non- reflective magnetic plasma configurations. Astronomy Astrophysics, 600:A44, 2018.
[23] G. L. Withbroe and R. W. Noyes. Mass and energy flow in the solar chromosphere and corona.Ann.Rev. Astron. Astrophys., 15:363–387, 1977. doi:10.1146/annurev.aa.15.090177.002051.
[24] R. Soler, J. Terradas, R. Oliver, J. L. Ballester,and M. Goossens. Kelvin-Helmholtz Instability in Coronal Magnetic Flux Tubes due to Azimuthal Shear Flows.ApJ, 712:875–882, April 2010
[25] S. W. McIntosh and B. De Pontieu. Estimating the "Dark" Energy Content of the Solar Corona. ApJ, 761:138, December 2012.
[26] M van Noort, L Rouppe van der Voort, and M. G. Löfdahl. Solar Image Restoration By Use Of Multi-frame Blind Deconvolution With Multiple Objects And Phase Diversity. Sol. Phys., 228:191–215, May 2005. doi: 10.1007/s11207-005-5782-z.
[27] K. P. Reardon and F Cavallini. Characterization of Fabry-Perot interferometers and multi-etalon transmission profiles. The IBIS instrumental profile.A&A, 481:897–912, April 2008. doi:10.1051/0004-6361:20078473.
[28] Fisher, Ronald A. (1971) [1935]. The Design of Experiments (9th ed.). Macmillan. ISBN 0-02-844690-9.
[29] Linnell Nemec, A. F., & Nemec, J. M. (1985). A test of significance for periods derived using phase-dispersion-minimization techniques. The Astronomical Journal, 90, 2317-2320.
[30] E. O'Shea, D. Banerjee, J. G. Doyle, B. Fleck, F. Murtagh, Active region oscillations, A&A 368 (3) 1095-1107 (2001) DOI: 10.1051/0004-6361:20010073
[31] Torrence C, Webster PJ. 1999, Interdecadal Changes in the ENSO Monsoon System. Journal of Climate, 12(8):2679–2690. ISSN0894-8755.
[32] D. J. Pascoe, A. N. Wright and I De Moortel. Coupled Alfvén and Kink Oscillations in Coronal Loops. The Astrophysical Journal, 711(2):990-996, Feb 2010.

[33] J. E.Vernazza, E. H.Avrett and R Loeser Structure of the solar chromosphere. III - Models of the EUV brightness components of the quiet-sun. The Astrophysical Journal, 5:635–725, April 1981
[34] H. Socas-Navarro, J. de la Cruz Rodríguez, A. Asensio Ramos, J. Trujillo Bueno, B. Ruiz Cobo, An open-source, massively parallel code for non-LTE synthesis and inversion of spectral lines and Zeeman-induced Stokes profiles, A&A 577 A7 (2015), DOI: 10.1051/0004-6361/201424860
[35] M. Goossens , R. Soler , J. Terradas, T. Van Doorsselaere, and G. Verth, THE TRANSVERSE AND ROTATIONAL MOTIONS OF MAGNETOHYDRODYNAMIC KINK WAVES IN THE SOLAR ATMOSPHERE, ApJ, 788, 9 (2014) DOI:10.1088/0004-637X/788/1/9
[36] https://warwick.ac.uk/fac/sci/physics/research/cfsa/research/wpc/vis/fast_m1_b0_running/trans also see for details https://warwick.ac.uk/fac/sci/physics/research/cfsa/research/wpc/vis/

Supplemental material

Data Set and Methods

The data of this study were acquired on 15th October 2008, commencing at 16:30 UT, with the IBIS instrument at the DST. The observations combined high-spectral resolution with short exposure times and a large field-of-view. The region presented here is AR 11005 which manifested as a small pore with a light bridge at a latitude [25.2° N, 10.0° W]. This dataset consists of 80 sequences of measurements, each containing a 21-point-scan of the Fe I 617.3 nm line with full Stokes profiles. The difference in wavelength between the sampled points of the Fe I line was 0.002 nm and the exposure time for each image was set to 80 ms, and each spectral scan took approximately 52 s to complete. These narrow-band data collected by the 1024×1024 pixel CCD camera were binned into 2 × 2 pixels giving a final pixel scale of these 512 × 512 images as 0.167 arcsec. For each narrow-band image, we also acquired a broad-band white light (WL; 621.3 ± 5 nm) counterpart, imaging the same field-of-view. The pixel scale of the 1024 × 1024 WL image was set at 0.083 arcsec and the exposure time was 80 ms. Each WL exposure was precisely aligned to the exposures of the narrow-band images through the shared use of a single shutter. Simultaneous WL images are used as a reference frame for the restoration of spectral images with the Multi-Frame Blind Deconvolution (MFBD) [26].
The reduction pipeline takes care of normal calibration processes (dark frames, flat fielding, etc.) and also corrects for blue-shift effects [27] and instrumental polarization. Residual cross-talks are reduced down to the noise level of the images, thus their effects can be safely neglected. In order to limit thermal effects, the local continuum Ic is chosen to normalise the spectral profiles. The photospheric Fe I data were used to estimate the total circular polarization (CP). This yields a map of CP for every frame in the data sequence. We remark that CP signals can be attributed to the line-of-sight (LOS) magnetic field. Before analysing the torsional oscillations, the residual tip-tilt motion was removed by means of a FFT cross-correlation technique with subpixel accuracy.

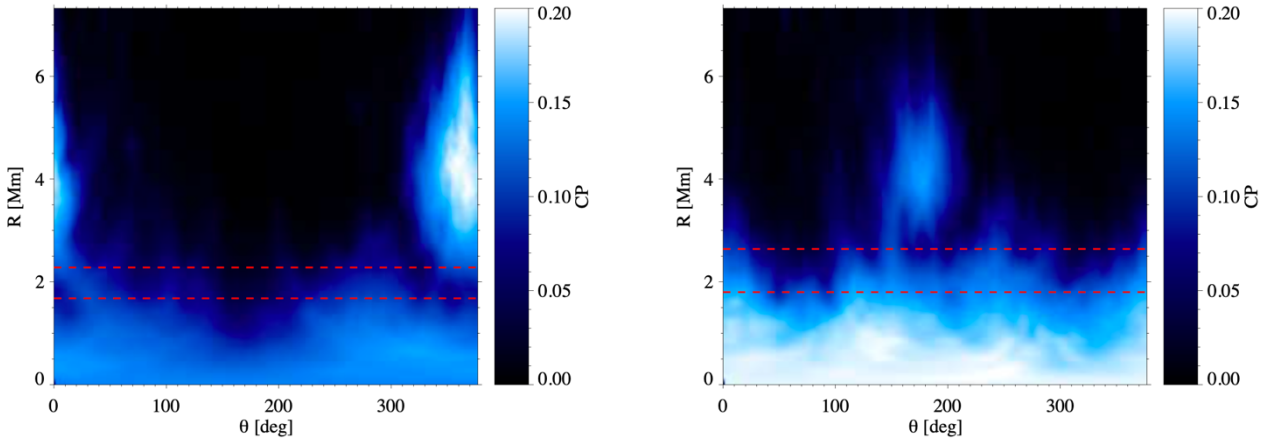

Supplementary Figure S1: Circular polarization maps and cross-correlation in polar coordinates.
Circular polarization maps of the left (left panel) and right (right panel) lobes of SEP polar coordinates, centred on the red crosses indicated in Fig. 2, 30 minutes after the start of acquisition. The dashed horizontal lines mark the region taken into account for the identification of the torsional displacement of the structures and denote the boundaries of the magnetic region.

The analysis of the calibrated data consisted of the simple strategy of plotting the circular polarization maps in polar coordinates (see Fig. S1). At each temporal step, the two lobes composing the magnetic structure are mapped into polar coordinates with origins at the approximate centres indicated by the

red crosses of Fig. 1 (main text). The exact position of the centre of each lobe is chosen as the one maximizing the amplitude of the observed oscillations. In the CP polar maps a band enclosing the boundary of the magnetic structure is chosen. After that, an FFT (Fast Fourier Transform) correlation is used to estimate the torsional displacement of the flux tube which manifests as a horizontal shift of this part of the polar maps in consecutive temporal steps. It is worth noting here that the estimation of the angular displacement of the two lobes of the magnetic structure simply reduces to the tracking of the boundaries of the structure itself. In Fig. 1 (main text) the angular oscillations of the two regions of the magnetic structure are shown as a function of time. In doing this, the average value of the time series is subtracted to better visualize the fluctuations with respect to the average itself.
Finally, the significance of the power peaks in the spectra was proven through a randomization test [28, 29]. This approach was already used in the past for the significance estimation of oscillations in the solar atmosphere (see for instance [30]). This technique relies on the random reshuffling of the time series in order to destroy temporal correlations. This process is performed several times, 1000 in our case, in order to assess the probability of the randomized time series to confirm the actual peaks of the spectrum that is assessed.
In order to study the spacing of the harmonics in Fig. 2, we consider the cross spectrum of the two time series (Fig. S2). In this plot, we perform a multi-gaussian fit of the peaks for which at least one of the two time series has a significance larger than 95%. This is done in order to guarantee the reliability of the result and to reject peaks that may be the result of noise.

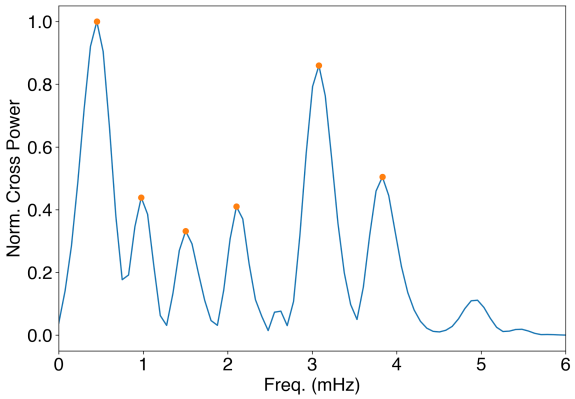

Supplementary Figure S2: Cross spectrum of the torsional oscillations.
Cross spectrum of the rotational velocity of the two lobes of the pore. The orange dots represent the peaks for which at least one of the two time series has a significance larger than 95%. These peaks are therefore the ones used in the multi-gaussian fit of the components of the spectrum to study their spacing (see Fig. 2).

In addition to the standard Fourier-based spectral analysis of the torsional oscillations, we also performed a wavelet analysis. For this purpose we have used the code described in [31].
The results of this analysis are shown in Fig. S3. Consistently with the results of the Fourier analysis, here we see the excitation of several periodicities with high confidence level (> 95%). In this figure, we also highlight the regions of the diagrams where a large coherence (>80%) between the two time series is observed (yellow dashed lines). This supports the scenario in which the two oscillations are the manifestation of the same mode as can be also seen directly by the anti-phase behaviour of the time series in Fig. 1.

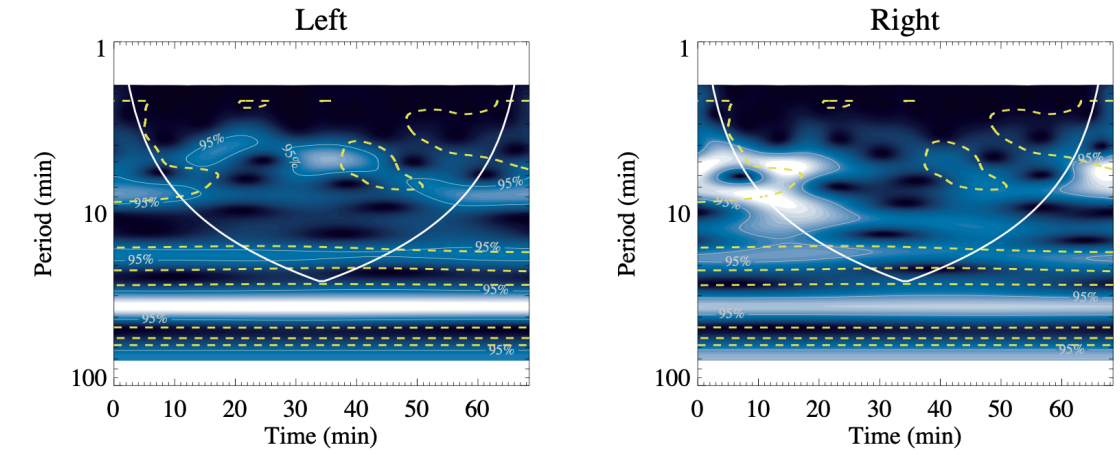

Supplementary Figure S3: Wavelet analysis of the rotational velocity of the two lobes.
Wavelet diagram of the torsional velocity of the two lobes. The two time series are normalized by their standard deviation. The white contours represent the 95% confidence levels and the yellow dashed lines highlight the regions of the period-time diagram where the two time series have a coherence larger than 80%. The white solid contour represents the cone-of-influence, which highlights the region where the estimated periodicities are less affected by edge effects (i.e. inside the cone).

MHD Simulations

A series of state-of-the-art 3D MHD simulations were performed using Lare3d to demonstrate a possible formation mechanism for m=1 torsional Alfvén waves in the lower solar atmosphere. Lare3d is a Lagrangian remap code that solves the resistive MHD equations over a 3D staggered grid [19].
A high-density, vertically stratified, divergent, flux tube is placed in the centre of the domain, representing the magnetic pore, and TAWs are then driven from the lower boundary, representing the observed photospheric surface.
The simulations performed are analogue to those presented in [32] with the very important distinction that here the domain is the chromosphere rather than the corona. A non-zero plasma-beta of order unity is therefore used across the domain and chromospheric temperatures and densities are employed [33].

$$B_{0r} = B_0 e^{-z/H} J_1(r/H),$$
$$B_{0z} = B_0 e^{-z/H} J_0(r/H),$$

The simulations were run over a grid with a resolution of 200 x 200 x 150, the dimensions of the domain are 8 Mm x 8 Mm x 3 Mm, with velocity perturbations exponentially damped in the upper 1 Mm of the domain to avoid wave reflection from the upper boundary. The initial conditions prescribe a static equilibrium with a constant pressure and an axisymmetric exponentially divergent potential magnetic field. The magnetic field used is given by [33], and is defined by the magnetic field in the radial and upward directions: where the characteristic value of the magnetic field B_0 =100 G. The magnetic scale height H = 10 Mm and J_0 and J_1 are Bessel functions of the first kind and of zero and first order, respectively. This magnetic field configuration is shown in Figure S4.

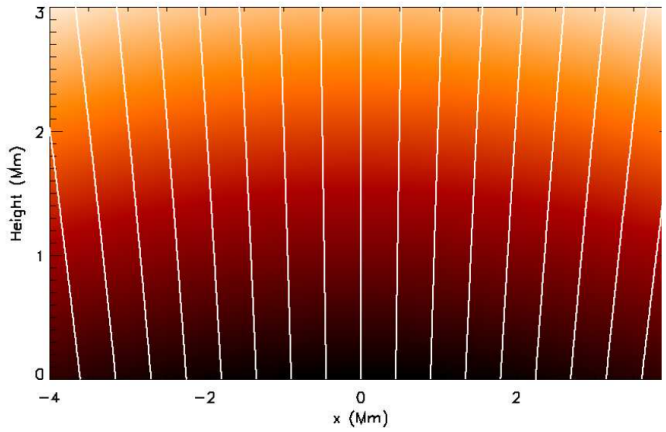

Supplementary Figure S4: Magnetic field configuration in the simulation domain.
A diagram of a typical magnetic field configuration shown as a vertical slice of the field through the central origin. The white lines represent the magnetic field lines whilst the shading is the magnetic field potential.

The initial density and temperature profiles are defined by,

$$\rho_0(r,z) = \rho_{00} e^{-z/H}(2 - \tanh(r - R)),$$
$$T(r,z) = \beta_0 \mu_m B_0^2 / 2\mu_0 k_B \rho(r,z)$$

where the characteristic density $\rho = 10^{-4}$ kg m^{-3}, the tube radius R = 2 Mm, the reduced mass μ_m=0.5 assuming a fully ionised plasma. The initial density and temperature profiles are shown in Figure S5.
The gas pressure is constant, $P_0 = \beta_0 B_0^2 / 2\mu_0$ and the plasma-beta is $\beta = \beta_0 (B_0^2/B^2)$, where β_0=1. It can be shown that given a scale height of H=10 Mm, β is never less than $\beta_0/2$ across the domain.
Alfvén waves are driven from the lower photospheric boundary of the domain throughout the simulations, the waves are driven across the photospheric boundary not just within the flux tube. The waves are driven in the transverse *y*-direction at three typical frequencies, corresponding to the frequencies observed, 0.45 mHz, 1.35 mHz and 2.25 mHz. The form of these perturbations are

$$v_y = a_0 f(t),$$
$$b_y = B_y - a_0 f(t)\sqrt{\rho_0},$$
$$f(t) = \sin(\omega t) + \sin(3\omega t) + \sin(5\omega t),$$

where v_y and b_y are the velocity and magnetic field perturbations, respectively, a_0 is the wave amplitude, $f(t)$ is the wave driving, B_y is the equilibrium magnetic field in the *y*-direction and the frequency is ω = 0.45 mHz. The driving amplitude for the velocity is a_0 = 0.223 km/s and the driving amplitude for the magnetic field is 43.3 G.

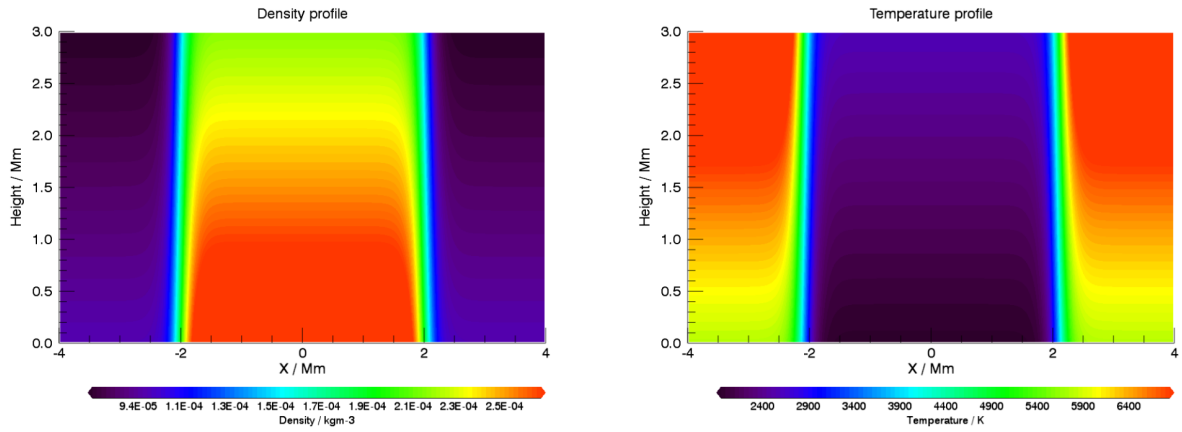

Supplementary Figure S5: Density and temperature profiles in the simulation domain.
Initial density (left) and temperature (right) profiles for the simulation shown as a vertical slice through the central origin. Density decreases exponentially with height and temperature increases exponentially with height. The denser, cooler flux tube is in the centre of the domain.

By a simulation time of approximately 20 minutes, a typical computation reaches a quasi-equilibrium with wave driving. Simulations were each run for a total 112 minutes.
At the density inhomogeneity at the edge of the flux tube transverse wave modes are coupled to the m =1 torsional Alfvén mode through resonant damping similar to the coupling of kink modes to the m =1 Alfvén mode described in [33]. A typical result shown here demonstrates the formation of two counter-rotating oscillations either side of the flux tube.
The oscillations in the velocity and magnetic fields at a height of 500 km above the photosphere are shown in Figure S6. In these figures, the two counter-rotating oscillations in the velocity and magnetic fields are readily identifiable. Supplementary animations have also been developed that reveal the dynamics of these oscillations; these movies can be found in the Supplementary Material.

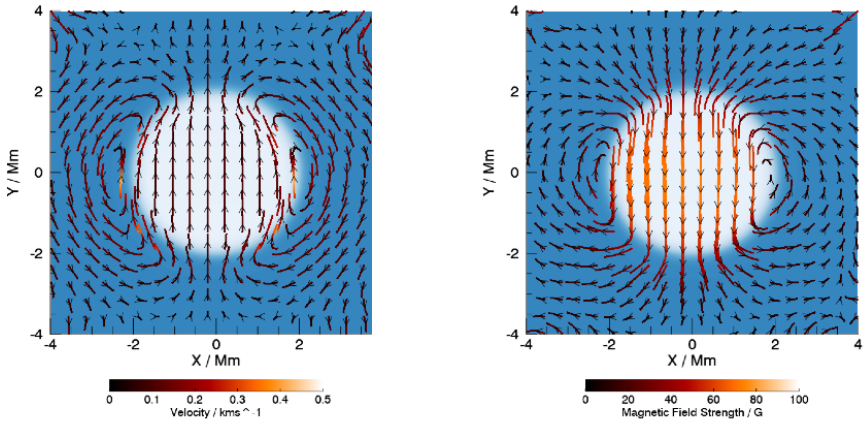

Supplementary Figure S6: Horizontal velocity and magnetic field perturbations.
Plots showing transverse perturbations to the velocity (left) and magnetic field (right) at 500 km above the photosphere. The perturbations are represented as partial streamlines and partial field lines respectively. The blue background shading is a density contour showing the position of the higher density flux tube in the centre of the domain.

Following these initial results, the simulations were repeated with a wider domain of 16 Mm x 16 Mm x 3 Mm in order to capture the torsional waves as part of the wider magnetic structure. The oscillations in the velocity and magnetic fields, at a height of 500 km above the photosphere, are shown for this simulation in Figure S7, in this case over a contour of the magnetic field strength. These images confirm that the torsional Alfvén waves are contained within a region of higher magnetic field strength, just as found in the observations.

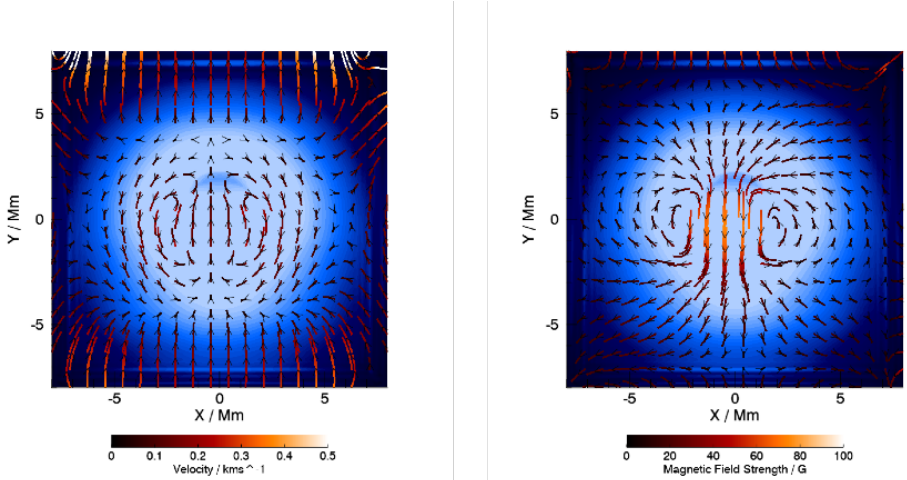

Supplementary Figure S7: Horizontal velocity and magnetic field perturbations over magnetic field contour.
Plots showing transverse perturbations to the velocity (left) and magnetic field (right) at 500 km above the photosphere. The perturbations are represented as partial streamlines and partial field lines respectively. The background shading is a magnetic field strength contour showing the position of the torsional waves within the central region of higher magnetic field strength.

The results demonstrate a formation mechanism for the pair of large scale non-axisymmetric torsional Alfvén modes detected in the chromosphere. The simulation shows that $|m=1|$ Alfvén modes like those detected can be generated from simple transverse plasma oscillations at the photosphere interacting with an inhomogeneity such as a higher density magnetic flux tube.

Energy flux estimate

In order to estimate the energy flux without making use of any assumption or model, the magnetic field and the plasma density values are estimated directly from the data. While the magnetic field is estimated using the COG method [22], the plasma density is estimated from spectropolarimetric inversions performed with the NICOLE code [34]. In the latter case, since the spectropolarimetric inversions can be spatially and temporally noisy, we take the temporal average of the density maps over the whole data set duration.

In addition, the magnetic field and plasma density are estimated in the annular regions considered in the cross-correlation. In particular, we derive the average value of both parameters in the two annular regions. The probability density functions of B and plasma density are shown in Fig. S8.

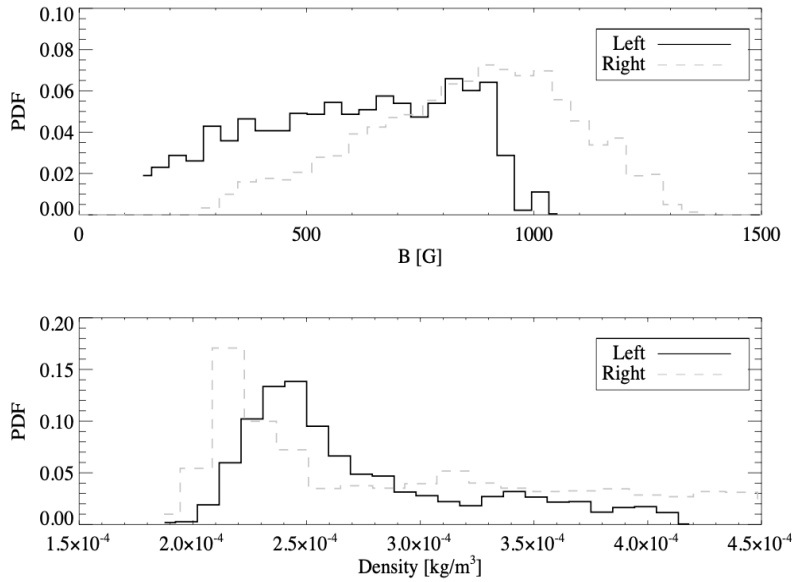

Supplementary Figure S8: Estimated density and magnetic flux in the magnetic pore.
Probability density function of B (upper panel) and plasma density (lower panel) in the two annular regions considered.
